# 3D printing of photocurable poly(glycerol sebacate) elastomers



2016 Biofabrication 8 045004

(http://iopscience.iop.org/1758-5090/8/4/045004)

Biofabrication

RECEIVED
26 July 2016

REVISED
20 August 2016

ACCEPTED FOR PUBLICATION
14 September 2016

PUBLISHED
10 October 2016

PAPER

# 3D printing of photocurable poly(glycerol sebacate) elastomers

**Yi-Cheun Yeh**[1,3], **Christopher B Highley**[1,3], **Liliang Ouyang**[1,2] **and Jason A Burdick**[1]

[1] Department of Bioengineering, University of Pennsylvania, Philadelphia, PA, USA
[2] Department of Mechanical Engineering, Tsinghua University, Beijing, People's Republic of China
[3] These authors contribute equally to this work.

**E-mail:** burdick2@seas.upenn.edu

**Keywords:** 3D printing, biodegradable, photopolymerization, elastomer, tissue engineering

## Abstract

Three-dimensional (3D) printed scaffolds have great potential in biomedicine; however, it is important that we are able to design such scaffolds with a range of diverse properties towards specific applications. Here, we report the extrusion-based 3D printing of biodegradable and photocurable acrylated polyglycerol sebacate (Acr-PGS) to fabricate scaffolds with elastic properties. Two Acr-PGS macromers were synthesized with varied molecular weights and viscosity, which were then blended to obtain photocurable macromer inks with a range of viscosities. The quality of extruded and photocured scaffolds was dependent on the initial ink viscosity, with flow of printed material resulting in a loss of structural resolution or sample breaking observed with too low or too high viscosity inks, respectively. However, scaffolds with high print resolution and up to ten layers were fabricated with an optimal ink viscosity. The mechanical properties of printed scaffolds were dependent on printing density, where the scaffolds with lower printing density possessed lower moduli and failure properties than higher density scaffolds. The 3D printed scaffolds supported the culture of 3T3 fibroblasts and both spreading and proliferation were observed, indicating that 3D printed Acr-PGS scaffolds are cytocompatible. These results demonstrate that Acr-PGS is a promising material for the fabrication of elastomeric scaffolds for biomedical applications.

## 1. Introduction

Three-dimensional printing (3DP) techniques possess great potential to fabricate constructs with defined and reproducible structures to meet widespread biomedical needs [1, 2]. 3D printed constructs are generated with well-established technologies that build up structures through approaches that typically deposit, cure, or solidify materials, one layer upon the next. Printing technologies (e.g., extrusion, ink-jetting, laser-directed fusion, and stereolithography) have been widely used in tissue engineering [3–7]. These approaches are capable of printing large macroporous constructs at high resolution and with complex and heterogeneous structures, such as towards the fabrication of patient-defined scaffolds for tissue repair. However, a major limitation towards the use of 3DP for many biomedical and tissue engineering applications is the limited availability of printable materials appropriate to a given application [8].

The biochemical and biophysical properties of 3DP constructs are primarily defined by the nature and chemistry of materials using in the 3DP process [9]. However, materials applied to 3DP approaches are constrained by the printing technology. In extrusion-based 3DP, for example, a printable material (ink) must flow through a nozzle and, upon leaving the nozzle, stabilize to preserve the printed structure. The development of inks has included traditional biodegradable polymeric materials (e.g., polylactic acid [10, 11], poly($\varepsilon$-caprolactone) [12, 13] and polylactic-co-glycolic acid [14] that have long been of interest in tissue engineering applications, as well as hydrogel inks based on natural (e.g., collagen [15, 16], gelatin [17, 18], alginate [19] and hyaluronic acid [20, 21]) and synthetic (e.g., poly(ethylene glycol) [22]) polymers.

Among these inks, the mechanical properties of polyester-based polymers do not match the elastic deformability of the extracellular matrix in many tissues in the body, and hydrogels often lack the strength necessary to bear loads in dynamic (e.g., muscle,

tendon, cartilage) and structural (e.g., ligament, skin) tissues. For example, scaffolds placed under long-term cyclic loading, as experienced in cardiac or cartilage tissues, risk either rapid failure upon loading or plastic deformation and ultimate failure. To address these limitations in material properties, inks that form elastomeric structures are needed; however, only a very few examples have been developed (e.g., polyurethanes) [23, 24].

Poly(glycerol sebacate) (PGS) is a tough, biocompatible, and biodegradable polymer, developed for *in vivo* applications where elastomeric properties are desirable [25–27]. PGS has tunable properties through changes in molecular weight and crosslinking, enabling the design of properties to suit a given application [28–30], and can be functionalized with bioactive molecules when needed [31]. Furthermore, the acrylation of the PGS prepolymer allows for PGS to be photocurable, simplifying the processing of PGS materials in many *in vitro* [32] and *in vivo* [33] studies. Due to its unique material properties, PGS has been widely used for applications in biomedicine, including in the engineering of cardiac [34–37], vascular [38, 39], and nervous [40] tissue constructs, as well as in the delivery of drugs [41].

Here, we leveraged the strengths of PGS to enable the design and fabrication of biocompatible, biodegradable, and elastomeric constructs with 3DP. To develop a printable ink, the properties of acrylated polyglycerol sebacate (Acr-PGS) were varied to obtain a material that could be extruded and rapidly photocrosslinked to fabricate 3D printed structures with high fidelity to computer-aided designs. Printed PGS structures were porous, elastomeric, and cytocompatible, making them great candidates for tissue engineering applications.

## 2. Materials and methods

### 2.1. Materials

All chemicals were purchased from Sigma-Aldrich and used as received unless otherwise indicated.

### 2.2. PGS synthesis and characterization

*2.2.1. Synthesis of PGS prepolymer and Acr-PGS*

PGS prepolymer was synthesized according to the reported literature via the condensation reaction of equimolar amounts of glycerol (ThermoFisher Scientific) and sebacic acid [25]. The reagents were stirred at 120 °C under nitrogen flow for 2 h and then a vacuum of 12 mbar was applied for various amounts of time (36 h or 48 h) to obtain PGS prepolymers with different molecular weights (termed LMW_PGS and HMW_PGS).

For acrylation, the PGS prepolymer was dissolved in anhydrous methylene chloride (ThermoFisher Scientific) containing triethylamine (TEA, equimolar to acryloyl chloride), 500 ppm 4-methoxyphenol and 0.1 wt% 4-(dimethylamino) pyridine, as performed previously [32, 33]. The reaction flask was cooled to 0 °C under nitrogen flow for 10 min. Acryloyl chloride (1:10 v/v in methylene chloride) was added dropwise into the solution and then stirred at room temperature overnight. An additional 500 ppm 4-methoxyphenol was added to the reaction solution and methylene chloride was removed using a rotary evaporator. Ethyl acetate was used to dissolve the remaining viscous liquid and the solution was vacuum filtered to remove TEA salts. Ethyl acetate was then removed using a rotary evaporator to leave a viscous liquid, which was then dissolved in methylene chloride and stored at 4 °C.

Acr-PGS from LMW_PGS and HMW_PGS prepolymers yielded photocurable macromers of two different molecular weights, LMW_Acr-PGS and HMW_Acr-PGS, respectively. Blended samples of Acr-PGS were prepared immediately prior to use by mixing LMW_Acr-PGS and HMW_Acr-PGS in specified proportions. The photoinitiator 2,2-dimethoxy-2-phenylacetophenone (DMPA) was added to the samples in methylene chloride and the methylene chloride was removed with a rotary evaporator prior to use.

*2.2.2. Characterization of PGS prepolymer and Acr-PGS*

The chemical structures and molecular weights of PGS prepolymer and Acr-PGS macromer were verified using $^{1}$H nuclear magnetic resonance (Bruker Advance 360 MHz, Bruker) and gel permeation chromatography (GPC). The acrylation percentage was determined using the estimation that two of the three hydroxy groups present in glycerol reacted with the sebacic acid.

For GPC analysis, PGS prepolymer was dissolved in tetrahydrofuran (THF) at a concentration of 5 mg ml$^{-1}$. GPC was performed on a Perkin-Elmer Series 10 high-performance liquid chromatograph, equipped with an LC-100 column oven (25 °C), a Nelson Analytical 900 Series integration data station, a Shimadzu RID-10A refractive index (RI) detector, and three AM gel columns (a guard column, 500 Å, 10 $\mu$m and 104 Å, 10 $\mu$m). THF was used as an eluent at a flow rate of 1 ml min$^{-1}$ and the number-average molecular weights were determined with poly(methyl methacrylate) standards (American Polymer Standards).

*2.2.3. Rheological measurement*

Acr-PGS macromers were mixed with 0.5 wt% DMPA for polymerization. Dynamic oscillatory time sweeps were performed using an AR2000 stress-controlled rheometer (TA Instruments) with an ultraviolet light-guide accessory (SmartSwap™, TA Instruments) connected to an ultraviolet light source (Omnicure S1000, EXFO). The photopolymerization of Acr-PGS was carried out under exposure to UV light (365 nm, 10 mW cm$^{-2}$). Storage ($G'$) and loss ($G''$) moduli with time were monitored under 0.5% strain and 1 Hz,

using a cone and plate geometry (59 min 42 s (0.995°) cone angle, 20 mm diameter, 27 $\mu$m gap) at 25 °C. The viscosity of Acr-PGS macromers was determined by measuring the slope of the shear stress versus shear rate plot, measured under continuous flow (0.0–50.0 $s^{-1}$) and with an equilibration duration time of 15 s.

*2.2.4. Tensile testing*

Photocured Acr-PGS samples (~2 mm height, 5 mm diameter) were measured using a dynamic mechanical analyzer (Q800, TA Instruments) at a constant strain rate of 10% $min^{-1}$ in air at room temperature. The modulus was determined from the slope of the stress–strain curve between 10% and 20% strain. For tensile testing, photocured Acr-PGS samples were prepared as dog-bone shaped specimens (~1 mm height, overall length of 30 mm, and a narrowed section that was 10 mm long and 5 mm wide). Samples were loaded into textured grips on an Instron 5848 universal testing system (Instron Corp., 10 N load cell) and tested with a 0.01 N preload and uniaxial extension (10 mm $min^{-1}$) until failure. Force and displacement data were acquired during loading and analyzed computationally (MATLAB, MathWorks) to determine sample stresses (calculated as measured forces divided by cross-sectional areas), failure stresses (the maximum stresses achieved), failure strains (the strains at which the failure stresses were achieved), and elastic moduli (taken from the slopes from 40% to 50% of failure strains).

### 2.3. 3DP and imaging

A 3D printer adapted for deposition of materials by extrusion, described previously [20, 21], was used for printing PGS. Briefly, an extrusion system was built that allowed extrusion of materials from a syringe with the plunger driven by the stepper motor by modifying a commercially available 3D printer (Revolution XL, Quintessential Universal Building Devices). This extrusion system was mounted to the 3D printer's print head and G-code commands typically used to control printer motion were used to position the syringe needle and actuate extrusion. Standard 3DP software was used for controlling the printer (Repetier, Hot-World GmbH & Co.) and G-code commands were generated from 3D models (Slic3r, slic3r.org) or custom written. The density of material within printed structures was varied by controlling the amount of interior volume designated to be occupied by material (fill density setting, in Slic3r) during generation of the G-code, including 30% for low density (LD), 45% for medium density (MD), and 60% for high density (HD). Print speeds were specified such that the extrusion rate matched the print head translation during printing, which was typically 4 mm $s^{-1}$. All printed structures included vertical shells but not horizontal shells.

Dog-bone structures were printed using the same 3D geometry used for casting the tensile test samples as described above and scaffolds with complex shapes derived from anatomical structures were printed from respective 3D computer models. Specifically, Acr-PGS macromers (with 0.5 wt% DMPA) were loaded into glass syringes (Gastight syringes, Hamiliton Company) with affixed blunt tip 25 G needles that were 6 mm long. Syringes were loaded onto the 3D printer and printed at ambient temperature (approximately 23 °C) with continuous irradiation of the print area with UV light (10 mW $cm^{-2}$) during printing and for 5 min post-printing. Rectangular grid print patterns (10 mm on each side) were used to assess materials for printability, with alternating layers of parallel filaments rotated 90° relative to the previous. Isometric, triangular grid print patterns were also investigated, such that parallel filaments were deposited, with alternating layers of parallel filaments rotated 60° relative to the previous.

### 2.4. Scaffold characterization

PGS printed scaffolds were imaged using scanning electron microscopy (SEM, FEI Quanta 600 environmental scanning electron microscope). To analyze the density of material in printed scaffolds, samples were weighed, their bulk dimensions measured, and mass per volume calculated. These values were compared to cast samples to determine percent density. For degradation analysis, solid or 3DP PGS polymer disks (1 mm thick, 3 mm diameter) were prepared as described above. PGS disks were weighed, incubated in 1.5 ml of phosphate-buffered saline (PBS, pH 7.4), and placed on an orbital shaker at 37 °C for up to 8 weeks. At weekly intervals, the solution was replaced with fresh PBS. At each time point (2, 4, and 8 weeks), three samples of each scaffold type were removed, lyophilized (Freezone 4.5, Labconco), and weighed to determine mass loss. For tensile testing, 3DP PGS samples were prepared and analyzed as described above.

### 2.5. Cell culture and characterization of cell-seeded PGS scaffolds

NIH 3T3 fibroblast cells were cultured at 37 °C under a humidified atmosphere of 5% $CO_2$ in high glucose Dulbecco's Modified Eagle's Medium (4.5 g $l^{-1}$ glucose) containing 10% fetal bovine serum and 1% penicillin/streptomycin. For cell seeding, 3D-printed PGS scaffolds were sterilized by incubation in 70% ethanol for 30 min, washing with PBS, and incubation in serum-containing media for 24 h. As an initial test of cell adhesion and viability, 3T3 cell suspensions ($5 \times 10^4$ cells in 2 ml) were dripped onto 3DP PGS scaffolds (2-layer, 10 × 10 mm, height: 0.29 mm) in a 24-well cell culture plate by pipette. After 24 h, the cell-seeded scaffolds were transferred to new wells and

stained with calcein-AM (2 $\mu$M in PBS, Life Technologies) at room temperature for 20 min.

To assess cell proliferation, 3T3 cell suspensions ($1 \times 10^5$ cells ml$^{-1}$ in 100 $\mu$l) were dripped onto the top center of 3DP PGS scaffolds (10-layer, $10 \times 10$ mm, height: 1.45 mm) in a 24-well cell culture plate. The scaffolds were incubated for 2 h and then 2 ml of culture medium were added. After 24 h, the scaffolds were transferred to a non-tissue culture treated 12-well plate and assessed for metabolic activity for up to 4 d using an Alamar blue assay according to the manufacturer's protocol (Invitrogen Biosource, USA).

### 2.6. Statistical analysis

One-way analysis of variance followed by Tukey HSD post-hoc tests was performed on data sets to determine statistical significance of differences in mechanical testing, degradation, and cell proliferation. Significance was set at $P < 0.05$ with $^{*}$ or $^{**}$ indicating $P < 0.05$ or 0.01, respectively. Error bars are reported in figures as the standard deviation unless otherwise noted.

## 3. Results and discussion

### 3.1. Characterization of PGS prepolymer and Acr-PGS

PGS is attractive for biomedical applications because it is elastic, biocompatible, and biodegradable. The ability to process it into complex geometries across multiple length scales, as with 3DP, would further expand the utility of PGS. A photocurable version of PGS, through the synthesis and reaction of Acr-PGS, allows for the fabrication of PGS materials through numerous fabrication techniques. Here, Acr-PGS met the requirements for extrusion-based 3DP—it is capable of flow during extrusion and then can rapidly stabilize during deposition using a photopolymerization reaction.

PGS prepolymers were first synthesized using a polycondensation reaction of glycerol and sebacic acid in a 1:1 molar ratio, where PGS prepolymer with either low molecular weight (LMW_PGS, $M_n = 5.78$ kDa, PDI = 1.78) or high molecular weight (HMW_PGS, $M_n = 6.32$ kDa, PDI = 1.99) was obtained with reaction times of 36 h and 48 h, respectively. Next, the hydroxyl groups of PGS were reacted with acryloyl chloride to obtain Acr-PGS with an acrylation of ~15% (figure 1(a)). Acr-PGS was photopolymerized by introducing initiator (0.5 wt% DMPA) and exposing to ultraviolet light. Rheology showed rapid polymerization of both LMW_Acr-PGS and HMW_Acr-PGS, where the crossover of the storage ($G'$) and the loss ($G''$) moduli occurred within seconds and a plateau modulus was reached within ~1 min (figure 1(b)). The storage modulus at the plateau was dependent on the Acr-PGS molecular weight, with ~8 kPa and ~57 kPa achieved with LMW_Acr-PGS and HMW_Acr-PGS, respectively. The ability to rapidly crosslink permits the eventual application of these materials to a 3DP process with photocuring for material stabilization.

### 3.2. 3DP of Acr-PGS macromers

Towards 3DP, the viscosity of the extruded ink is important in both the ability to extrude a continuous material and to maintain the printed structure during stabilization, in this case with photopolymerization. Here, the Acr-PGS molecular weight was altered by changing the condensation polymerization time prior to acrylation, which led to materials with measured viscosities of either 3.18 or 8.78 Pa s for LMW_Acr-PGS and HMW_Acr-PGS, respectively (figure 2(a)). Furthermore, a range of Acr-PGS viscosities between these limits were achieved through simple blending of LMW_Acr-PGS and HMW_Acr-PGS at ratios of 50/50, 25/75, and 10/90. As expected, with increasing HMW_Acr-PGS content, the sample viscosity also increased (figure 2(a)).

Tests to assess the printability of these formulations included the 3DP of rectangular grid print patterns to a height of four layers in the $z$-direction under continuous UV irradiation (figure 2(b)). Upon imaging the $xy$-planes of these printed structures from above, the rectangular pores in the 100/0 and 50/50 samples were observed to be partially occluded with material and the intersections of filaments in the 25/75 sample also showed pooling of material. The printing of the more viscous 0/100 macromer led to irregular, relatively narrow filaments with some material fracture. Thus, macromers with too low of viscosity lost their printed structure prior to stabilization, whereas a material that was too viscous led to fracture and the inability to form continuous filaments. However, likely due to an optimal viscosity, the 10/90 sample maintained high fidelity to the computer-aided design, with regular filament widths, regular spacing, and no evidence of material pooling at intersections. When the 10/90 sample was printed without UV irradiation, pore occlusion was observed, illustrating the importance of rapid stabilization prior to flow of the material.

The optimal viscosity for extrusion-based printing depends on numerous parameters, such as the needle size and the speed of stabilization. Thus, the viscosity to be used may need to be designed for each printing system. We chose to blend two materials to alter the PGS macromer viscosity; however, this could also be done with a single macromer and optimized PGS prepolymer synthesis times if properties and structure-property relationships are known *a priori*. There may also be other methods available to alter the material viscosity, such as with a solvent, through heating of the nozzle during extrusion, or by introducing thixotropic agents; yet considerations to the removal of the

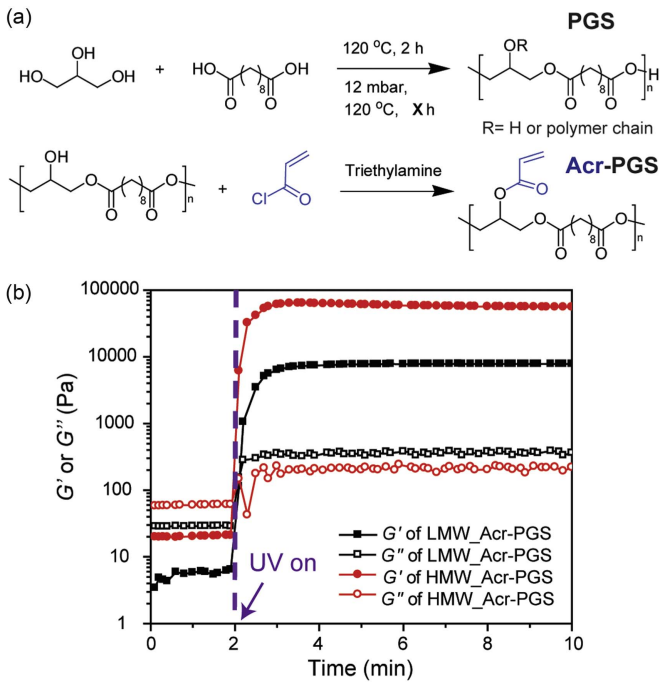


**Figure 1.** (a) Synthesis schemes of PGS prepolymer and Acr-PGS. (b) Rheology of the photopolymerization of LMW_Acr-PGS and HMW_Acr-PGS under UV exposure (10 mW $cm^{-2}$).

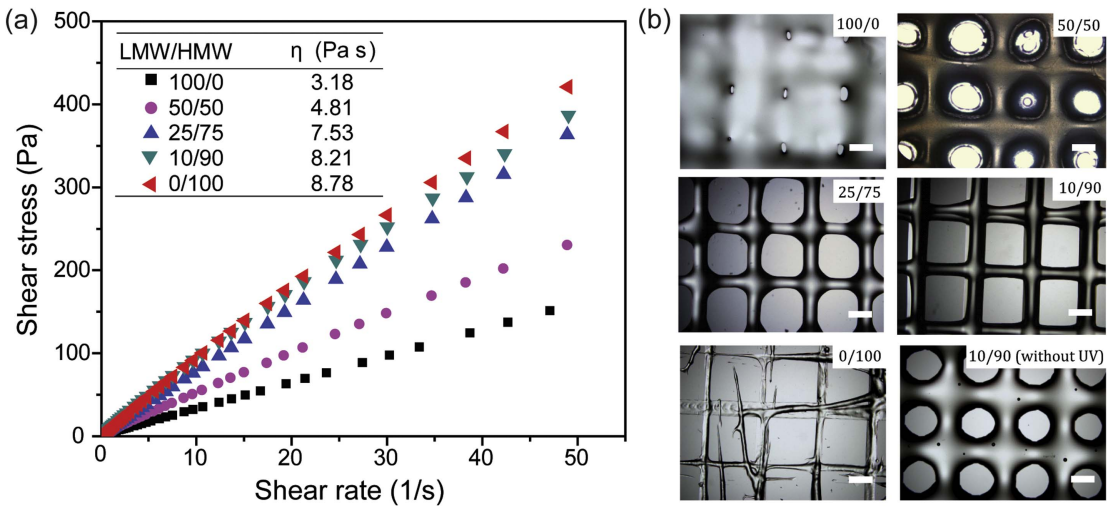


**Figure 2.** (a) Shear stress-shear rate plots of LMW_Acr-PGS/HMW_Acr-PGS blends with different ratios. (b) Printed filaments of LMW_Acr_PGS/HMW_Acr_PGS blends with different ratios and one formulation (10/90) without light exposure. Scale bars are 500 $\mu$m.

solvent, the influence of temperature on material stability, or the effects of a secondary material in the construct's final application would need to be addressed.

Using an isometric triangular grid pattern and the optimized 10/90 LMW_Acr-PGS/HMW_Acr-PGS formulation, four- and ten-layered structures were printed and examined for fidelity to computer-aided designs using light microscopy and SEM (figure 3). Both 4-layered (figure 3(a)) and 10-layered (figure 3(b)) structures showed uniform fibers, no pore occlusion and high precision filament deposition at points of intersection. Thus, highly regular structures could be achieved at the micro- and mesoscales in printing Acr-PGS macromers with subsequent photocuring. Characteristic of 3DP capabilities, here with stepper motor positioning specified for resolutions of 3.5 $\mu$m $\pm$ 5%, filaments could be repeatedly placed with great precision and at high resolution. The printed filaments had measured diameters of 258.8 $\pm$ 14.8 $\mu$m, but this can be changed through parameters such as needle gauge and printing speed.

Printing to 10 layers provided indirect evidence that printed Acr-PGS experienced minimal collapse during the printing of numerous layers. Also, minimal

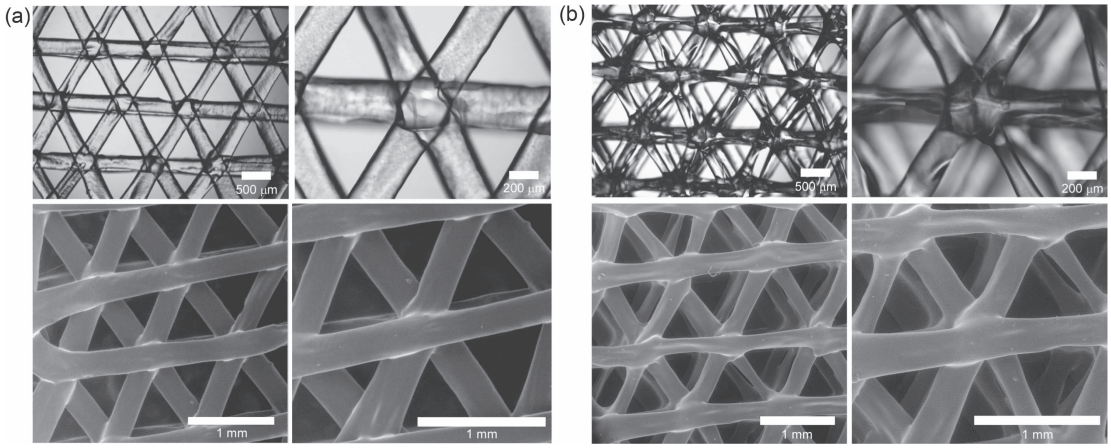


**Figure 3.** (a) 4-layered and (b) 10-layered printed patterns using 10/90 LMW_Acr-PGS/HMW_Acr-PGS blends. The top images are optical images, and the bottom images are SEM images.

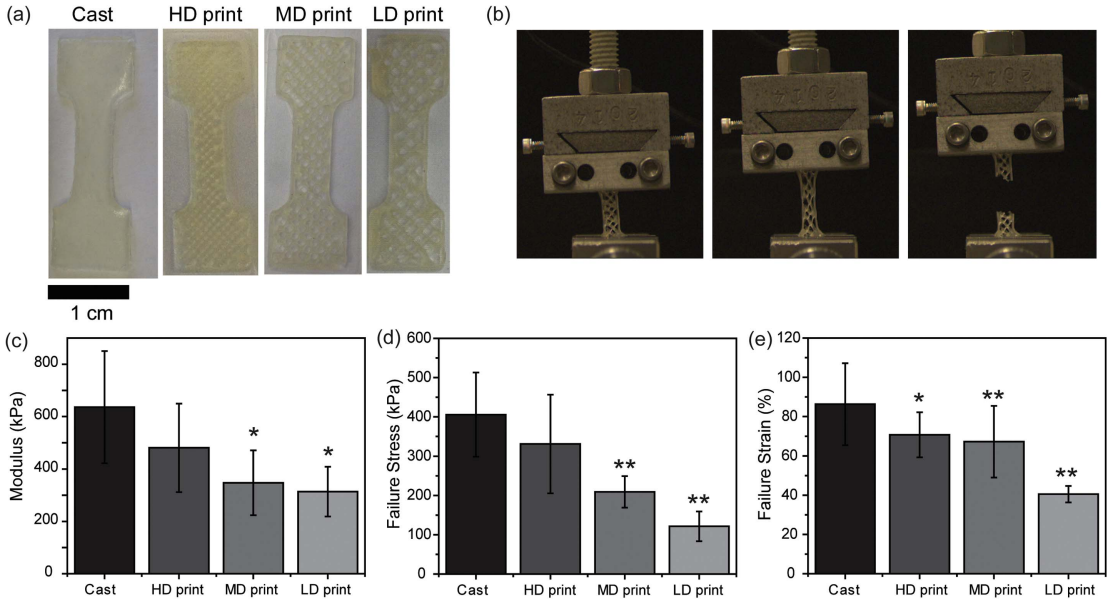


**Figure 4.** (a) Cast and printed PGS samples with different printing material density for tensile testing. (b) Representative images of a low-density printed sample immediately before, during, and after tensile loading. (c) Modulus, (d) failure stress and (e) failure strain of the cast and printed samples at various densities. ($n \geqslant 4$ measurements per group, data presented as mean $\pm$ s.d.). Statistical significance was calculated based on printed samples relative to cast sample. $^{*}P < 0.05$ and $^{**}P < 0.01$.

pooling was observed at the intersections of filaments, which would have indicated material flow downward in the *z*-direction prior to stabilization. SEM images revealed distinct filaments in the *z*-direction, which are joined at points of intersection, but do not coalesce between intersections to parallel strands in lower layers. This formulation therefore allowed for the filaments to be stabilized by covalent crosslinking prior to downward flow or significant sagging along the length of the filament spans. This is desirable for the application of these 3D printed constructs in tissue engineering, where the diffusion of nutrients, wastes, and signaling molecules as well as migration throughout the scaffold is important.

### 3.3. Mechanical and degradation analysis of 3DP scaffolds

Samples of cast and 3DP Acr-PGS, prepared with the 10/90 LMW/HMW PGS mixture, were used for uniaxial tensile testing (figures 4(a) and (b)). Printed samples had no continuous bottom or top layer, but instead consisted of a wall and a rectilinear infill whose fill density was varied to assess how macroscale construct properties might be affected by varying the mesoscale structure. Densities measured for printed samples, as a percentage of cast sample density, were 35.8% $\pm$ 3.6%, 49.7% $\pm$ 5.3%, and 60.0% $\pm$ 4.7% ($n = 3$, mean $\pm$ standard deviation), for the LD, MD, and HD samples, respectively. As expected, the measured properties of the scaffolds varied with

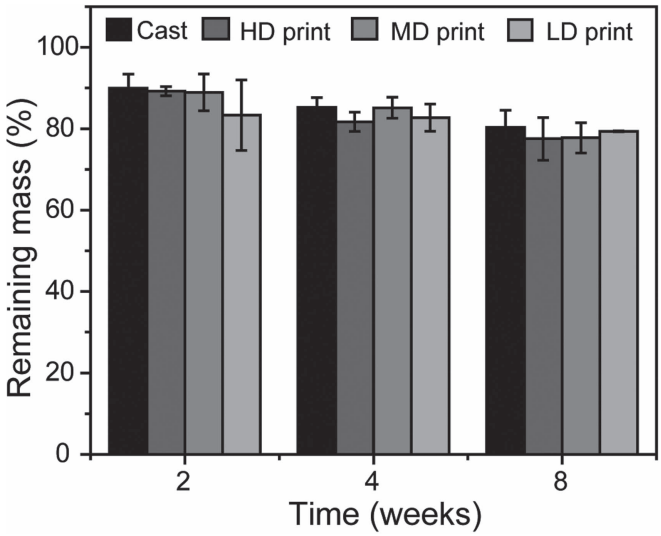


**Figure 5.** Mass loss of PGS scaffolds during incubation in PBS at 37 °C for up to 8 weeks. ($n = 3$ measurements per group, data presented as mean ± s.d.). There were no statistical differences in mass loss measured for any of the groups at these time points.

filament density (figures 4(c)–(e)). The highest modulus of ~740 kPa was observed for the cast sample, followed by the HD sample at ~480 kPa, the MD sample at ~350 kPa, and finally the LD sample at ~310 kPa (figure 4(c)). This trend was mirrored in measurements of failure stresses (figure 4(d)), with the cast sample failing at ~450 kPa, the HD sample at ~330 kPa, MD at ~210 kPa, and LD at ~120 kPa. Failure strains (figure 4(e)) followed a similar trend, measured at ~86% for the cast sample, ~70% for the HD sample, ~67% for MD, and then ~40% for the LD sample. Through 3DP, the properties of macroscale constructs were therefore modified by changes in their mesoscale structures.

Here, the tensile properties of the scaffolds varied to some extent via the density of the printed materials, while maintaining the same material formulation. This observation is consistent with expectations, as stresses were measured as a function of the macrostructural cross-section, whereas the actual construct was composed of discrete struts, which themselves were composed of layers of printed filaments, whose density was varied at the mesoscale. All materials exhibited some elasticity, as the materials were deformed prior to failure. In addition to printed filament density, there are numerous other methods that can be used to alter material mechanical properties. For example, the crosslink density could be altered through changes in the polymerization time or through alterations in the acrylation percentage of the Acr-PGS macromers.

In addition to mechanical properties, the degradability of the various PGS scaffolds was assessed *in vitro* in PBS for up to 8 weeks (figure 5). As expected based on previous studies of PGS degradation [42, 43], the materials degraded slowly, losing only ~20% of their mass over an 8 week period for all print densities. As PGS is known to degrade by surface erosion, these results would be expected given that increasing filament density should not alter the surface-to-volume ratio of the PGS material given the high porosity of the structures. While junction points between filaments would increase, filaments are otherwise in contact with water over their surface, and are expected to degrade at the same rate, regardless of how many are present. The independent relationship observed between degradation rates and material density should allow mesoscale features, such as filament density or placement, to be used to modify bulk properties of the construct without shortening or extending its lifespan. This may be useful in tissue engineering, by allowing different properties to be achieved during tissue regeneration without shortening the time over which the scaffold supports tissue regeneration. However, the degradation times could be altered through the synthesis of varied macromers, although this would be tied to mechanical properties.

### 3.4. 3DP of tissue structures

PGS constructs replicating the complex, macroscale geometry of the lateral meniscus of a knee (figure 6(a)) and an ear (figure 6(b)) were printed from 3D computer models. The printed constructs faithfully reflected the macroscale complexity of the 3D models and were elastically deformable. In printing, structural complexity can be controlled across length scales (micro <100 um, meso <5 mm, macro >5 mm), allowing properties to be governed by microscale features and to alter the porosity of printed structures. While experiments printing grid structures demonstrated the ability to print complex geometries and control material structure at the micro- and mesoscales using Acr-PGS, macroscale complexity will allow constructs to be printed that reflect biologically

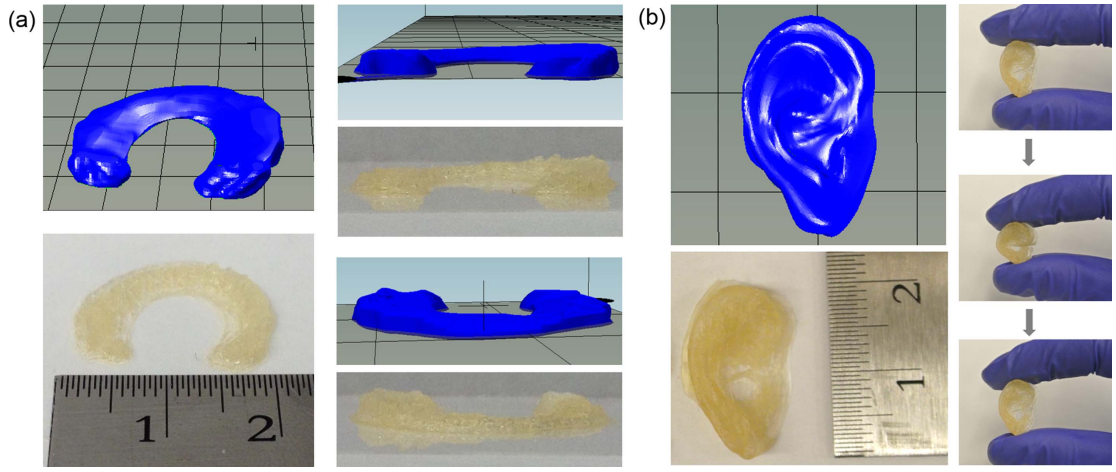


**Figure 6.** 3D-printed tissue structures based on the (a) lateral meniscus of a knee and (b) the cartilaginous structure of an ear. Printed structures replicate the image files, with internal porosity based on specified fill densities of 40%. Printed structures are elastic, deforming under applied forces and recovering fully.

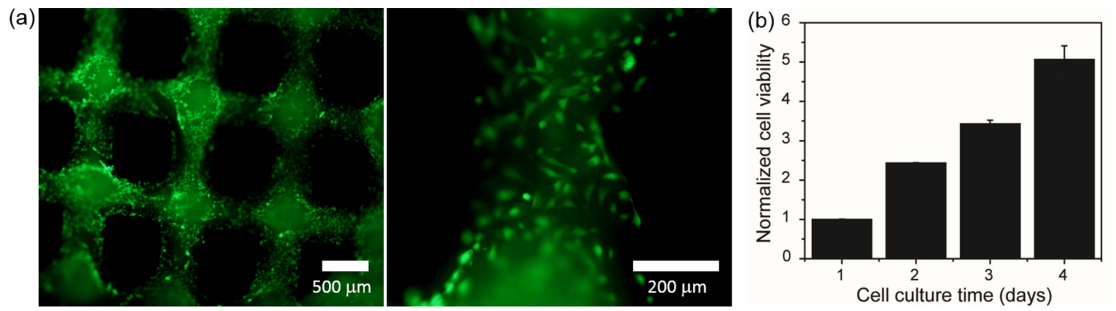


**Figure 7.** (a) 3T3 fibroblasts cultured on a 2-layered scaffold and stained with calcein-AM after culture for 24 h. (b) Normalized (to day 1 values) metabolic activity of 3T3 fibroblasts cells on a 10-layered scaffold, where activity was determined for up to 4 d using an Alamar blue assay. ($n = 3$ measurements per group, data presented as mean $\pm$ s.d.). The values at all time points were statistically significant from each other ($P < 0.001$ for all comparisons).

relevant and patient-specific geometries. Considering the high (>400 kPa) elastic moduli measured in tensile tests of Acr-PGS structures, these results demonstrate that it may be possible to 3D print scaffolds to aid in the replacement of tissues that are highly elastic or subject to significant and repeated loading *in vivo*, such as with the ear or the knee's lateral meniscus, respectively.

### 3.5. Cell culture and cytocompatibility

Towards applying 3DP PGS structures in regenerative medicine, it was important to show that they supported cell growth and proliferation. Cytocompatibility was assessed with both calcein AM staining of 3T3 fibroblasts seeded onto constructs (figure 7(a)) and metabolic assays that monitored cells for up to 4 d (figure 7(b)). The fibroblasts were observed to be viable and to spread into confluent layers when seeded onto the printed PGS filaments. These observations were expected, in accordance with observations reported elsewhere on cellular adhesion to PGS surfaces [26], likely mediated through serum adsorption to the polymer surfaces and integrin-mediated adhesion. Using Alamar blue to assay cellular metabolism, as a proxy for cell number, an increase in the number of fibroblasts was observed for the 3DP Acr-PGS constructs over time. At day 2, the cell population had doubled over day 1, and continued to increase up to day 4 (figure 7(b)). Cell proliferation was thus observed with doubling times on the order of the 20 h doubling time typically observed for 3T3 fibroblasts. It is not surprising that the 3DP process did not negatively affect PGS cytocompatibility, as the bulk material is the same as with previous studies.

## 4. Conclusions

The continual development of 3DP technologies will aid in the engineering of complex tissues. Here, we were able to 3D print Acr-PGS inks to harness the elastomeric, biodegradable, and cytocompatible properties of PGS into 3DP scaffolds. The design and control of PGS properties, including rheological and crosslinking behavior, through synthesis and ink formulation enabled the rapid fabrication of spatially

complex, elastomeric scaffolds. These scaffolds were demonstrated to have multiscale structures, capable of supporting cell cultures and replicating native tissue shapes, according to specified computer-aided designs. This first demonstration of the ability to 3D print PGS combines the strengths of 3DP and PGS, expanding the properties available in 3D printed structures and the potential to fabricate complex biocompatible, elastomeric tissue replacements.

## Acknowledgments

The authors would like to thank Dr Christopher B Rodell for assistance in tensile testing measurements and Dr Mojtaba Enayati and Professor Virgil Percec (Department of Chemistry, University of Pennsylvania) for assistance with GPC. This work was supported by an American Heart Association Established Investigator Award and a National Science Foundation MRSEC Award. LO acknowledges financial support from the China Scholarship Council (LO File 201506210148).

## References

[1] Zhu W, Ma X, Gou M, Mei D, Zhang K and Chen S 2016 3D printing of functional biomaterials for tissue engineering *Curr. Opin. Biotechnol.* **40** 103–12
[2] Sears N A, Seshadri D R, Dhavalikar P S and Cosgriff-Hernandez E 2016 A review of three-dimensional printing in tissue engineering *Tissue Eng.* B **22** 298-310
[3] Ozbolat I T and Hospodiuk M 2016 Current advances and future perspectives in extrusion-based bioprinting *Biomaterials* **76** 321–43
[4] Shirazi S F S, Gharehkhani S, Mehrali M, Yarmand H, Metselaar H S C, Kadri N A and Osman N A A 2015 A review on powder-based additive manufacturing for tissue engineering: selective laser sintering and inkjet 3D printing *Sci. Technol. Adv. Mater.* **16** 033502
[5] Melchels F P W, Feijen J and Grijpma D W 2010 A review on stereolithography and its applications in biomedical engineering *Biomaterials* **31** 6121–30
[6] Derby B 2012 Printing and prototyping of tissues and scaffolds *Science* **338** 921–6
[7] Mandrycky C, Wang Z, Kim K and Kim D-H 2016 3D bioprinting for engineering complex tissues *Biotechnol. Adv.* **34** 422-34
[8] Melchels F P W, Domingos M A N, Klein T J, Malda J, Bartolo P J and Hutmacher D W 2012 Additive manufacturing of tissues and organs *Prog. Polym. Sci.* **37** 1079–104
[9] Guvendiren M, Molde J, Soares R M D and Kohn J 2016 Designing biomaterials for 3D printing *ACS Biomater. Sci. Eng.* in press (doi:10.1021/acsbiomaterials.6b00121)
[10] Serra T, Planell J A and Navarro M 2013 High-resolution PLA-based composite scaffolds via 3D printing technology *Acta Biomater.* **9** 5521–30
[11] Serra T, Ortiz-Hernandez M, Engel E, Planell J A and Navarro M 2014 Relevance of PEG in PLA-based blends for tissue engineering 3D-printed scaffolds *Mater. Sci. Eng.* C **38** 55–62
[12] Seyednejad H, Gawlitta D, Kuiper R V, de Bruin A, van Nostrum C F, Vermonden T, Dhert W J and Hennink W E 2012 *In vivo* biocompatibility and biodegradation of 3D-printed porous scaffolds based on a hydroxyl-functionalized poly(ε-caprolactone) *Biomaterials* **33** 4309–18
[13] Shor L, Chang R, Güçeri S, Gondon J, Kang Q, Hartsock L, An Y and Sun W 2009 Precision extruding deposition (PED) fabrication of polycaprolactone (PCL) scaffolds for bone tissue engineering *Biofabrication* **1** 015003
[14] Chia H N and Wu B M 2015 High-resolution direct 3D printed PLGA scaffolds: print and shrink *Biofabrication* **7** 015002
[15] Inzana J A, Olvera D, Fuller S M, Kelly J P, Graeve O A, Schwarz E M, Kates S L and Awad H A 2014 3D printing of composite calcium phosphate and collagen scaffolds for bone regeneration *Biomaterials* **35** 4026–34
[16] Bell A, Kofron M and Nistor V 2015 Multiphoton crosslinking for biocompatible 3D printing of type I collagen *Biofabrication* **7** 035007
[17] Ouyang L, Yao R, Mao S, Chen X, Na J and Sun W 2015 Three-dimensional bioprinting of embryonic stem cells directs high-throughput and highly uniformed embryoid body formation *Biofabrication* **7** 044101
[18] Billiet T, Gevaert E, Schryver T D, Cornelissen M and Dubruel P 2014 The 3D printing of gelatin methacrylamide cell-laden tissue-engineered constructs with high cell viability *Biomaterials* **35** 49–62
[19] Tabriz A G, Hermida M A, Leslie N R and Shu W 2015 Three-dimensional bioprinting of complex cell laden alginate hydrogel structures *Biofabrication* **7** 045012
[20] Highley C B, Rodell C B and Burdick J A 2015 Direct 3D printing of shear-thinning hydrogels into self-healing hydrogels *Adv. Mater.* **27** 5075–79
[21] Ouyang L, Highley C B, Rodell C B, Sun W and Burdick J A 2016 3D printing of shear-thinning hyaluronic acid hydrogels with secondary crosslinking *ACS Biomater. Sci. Eng.* in press (doi:10.1021/acsbiomaterials.6b00158)
[22] Hockaday L A *et al* 2012 Rapid 3D printing of anatomically accurate and mechanically heterogeneous aortic valve hydrogel scaffolds *Biofabrication* **4** 035005
[23] Hung K-C, Tseng C-S and Hsu S-H 2014 Synthesis and 3D printing of biodegradable polyurethane elastomer by a water-based process for cartilage tissue engineering applications *Adv. Healthcare Mater.* **3** 1578–87
[24] Hung K-C, Tseng C-S, Dai L-G and Hsu S-H 2016 Water-based polyurethane 3D printed scaffolds with controlled release function for customized cartilage tissue engineering *Biomaterials* **83** 156–68
[25] Wang Y, Ameer G, Sheppard B and Langer R 2002 A tough biodegradable elastomer *Nat. Biotechnol.* **20** 602–6
[26] Loh X J, Karim A A and Owh C 2015 Poly(glycerol sebacate) biomaterial: synthesis and biomedical applications *J. Mater. Chem.* B **3** 7641–52
[27] Rai R, Tallawi M, Grigore A and Boccaccini A R 2012 Synthesis, properties and biomedical applications of poly(glycerol sebacate) (PGS): a review *Prog. Polym. Sci.* **37** 1051–78
[28] Jeffries E, Allen R, Gao J, Pesce M and Wang Y 2015 Highly elastic and suturable electrospun poly(glycerol sebacate) fibrous scaffolds *Acta Biomater.* **18** 30–9
[29] Ifkovits J L, Devlin J J, Eng G, Martens T P, Vunjak-Novakovic G and Burdick J A 2009 Biodegradable fibrous scaffolds with tunable properties formed from photo-cross-linkable poly(glycerol sebacate) *ACS Appl. Mater. Interfaces* **1** 1878–86
[30] Ravichandran R, Venugopal J R, Sundarrajan S, Mukherjee S, Sridhar R and Ramakrishna S 2012 Minimally invasive injectable short nanofibers of poly(glycerol sebacate) for cardiac tissue engineering *Nanotechnology* **23** 385102
[31] Wang S, Jeffries E, Gao J, Sun L, You Z and Wang Y 2016 Polyester with pendent acetylcholine-mimicking functionalities promotes neurite growth *ACS Appl. Mater. Interfaces* **8** 9590–99
[32] Nijst C L E, Bruggeman J P, Karp J M, Ferreira L, Zumbuehl A, Bettinger C J and Langer R 2007 Synthesis and characterization of photocurable elastomers from poly(glycerol-co-sebacate) *Biomacromolecules* **8** 3067–73
[33] Ifkovits J L, Padera R F and Burdick J A 2008 Biodegradable and radically polymerized elastomers with enhanced processing capabilities *Biomed. Mater.* **3** 034104

[34] Chen Q-Z, Bismarck A, Hansen U, Junaid S, Tran M Q, Harding S E, Ali N N, Aldo R. and Boccaccin A R 2008 Characterisation of a soft elastomer poly(glycerol sebacate) designed to match the mechanical properties of myocardial tissue *Biomaterials* **29** 47–57
[35] Chen Q-Z *et al* 2010 An elastomeric patch derived from poly (glycerol sebacate) for delivery of embryonic stem cells to the heart *Biomaterials* **31** 3885–93
[36] Pereira M J *et al* 2013 A highly tunable biocompatible and multifunctional biodegradable elastomer *Adv. Mater.* **25** 1209–15
[37] Rai R *et al* 2013 Biomimetic poly(glycerol sebacate) (PGS) membranes for cardiac patch application *Mater. Sci. Eng.* C **33** 3677–87
[38] Lee K-W and Wang Y 2011 Elastomeric PGS scaffolds in arterial tissue engineering *J. Vis. Exp.* **50** e2691
[39] Motlagh D, Yang J, Lui K Y, Webb A R and Ameer G A 2006 Hemocompatibility evaluation of poly(glycerol sebacate) *in vitro* for vascular tissue engineering *Biomaterials* **27** 4315–24
[40] Allen R A *et al* 2014 Nerve regeneration and elastin formation within poly(glycerol sebacate)-based synthetic arterial grafts one-year post-implantation in a rat model *Biomaterials* **35** 165–73
[41] Sun Z-J, Chen C, Sun M-Z, Ai C-H, Lu X-L, Zheng Y-F, Yang B-F and Dong D-L 2009 The application of poly (glycerol–sebacate) as biodegradable drug carrier *Biomaterials* **30** 5209–14
[42] Li X, Hong A T L, Naskar N and Chung H-J 2015 Criteria for quick and consistent synthesis of poly(glycerol sebacate) for tailored mechanical properties *Biomacromolecules* **16** 1525–33
[43] Frydrych M and Chen B 2013 Large three-dimensional poly (glycerol sebacate)-based scaffolds-a freeze-drying preparation approach *J. Mater. Chem.* B **1** 6650–61